ACS APPLIED MATERIALS & INTERFACES

Research Article

www.acsami.org

Microwave-Assisted Reactant-Protecting Strategy toward Efficient MoS_2 Electrocatalysts in Hydrogen Evolution Reaction

Ning Liu,[†,‡] Yulin Guo,[†,‡] Xiaoyun Yang,[‡] Huanlei Lin,[‡] Lichun Yang,[*,§] Zhangping Shi,[⊥] Zhiwei Zhong,[‡] Sinong Wang,[⊥] Yi Tang,[⊥] and Qingsheng Gao[*,‡]

[‡]Department of Chemistry, Jinan University, No. 601 Huangpu Avenue West, 510632 Guangzhou, P. R. China

[§]School of Materials Science and Engineering, South China University of Technology, No. 381 Wushan Road, 510641 Guangzhou, P. R. China

[⊥]Department of Chemistry, Shanghai Key Laboratory of Molecular Catalysis and Innovative Materials, Laboratory of Advanced Materials and Collaborative Innovation Center of Chemistry for Energy Materials, Fudan University, No. 220 Handan Road, 200433 Shanghai, P. R. China

Supporting Information

ABSTRACT: The exposure of rich active sites is crucial for MoS_2 nanocatalysts in efficient hydrogen evolution reaction (HER). However, the active (010) and (100) planes tend to vanish during preparation because of their high surface energy. Employing the protection by thiourea (TU) reactant, a microwave-assisted reactant-protecting strategy is successfully introduced to fabricate active-site-rich MoS_2 (AS-rich MoS_2). The bifunctionality of TU, as both a reactant and a capping agent, ensures rich interactions for the effective protection and easy exposure of active sites in MoS_2, avoiding the complicated control and fussy procedure related to additional surfactants and templates. The as-obtained AS-rich MoS_2 presents the superior HER activity characterized by its high current density (j = 68 mA cm^{-2} at −300 mV vs RHE), low Tafel slope (53.5 mV dec^{-1}) and low onset overpotential (180 mV), which stems from the rich catalytic sites and the promoted conductivity. This work elucidates a feasible way toward high performance catalysts via interface engineering, shedding some light on the development of emerging nanocatalysts.

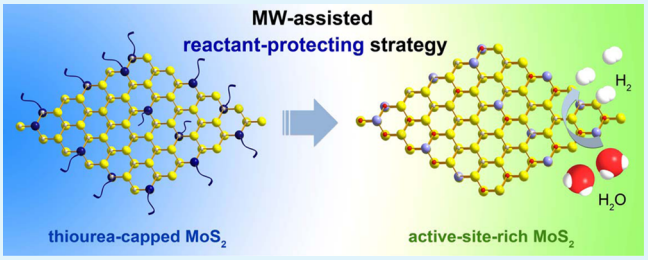

KEYWORDS: *hydrogen evolution, molybdenum disulfide, microwave, active sites, reactant-protecting*

INTRODUCTION

Hydrogen is considered as a clean energy carrier alternative to exhaustible resource.[1,2] And the electrochemical hydrogen evolution reaction (HER) from water has become a hotspot in sustainable hydrogen production, promoted by the booming technology for generating electricity from renewable resources (e.g., sunlight and wind).[3,4] Although noble metals, e.g., platinum, show high efficiency in electrochemical HER, the scarcity and high cost severely inhibit their practical application.[5−7] In this regard, advanced catalysts with element abundance, economic cost, and high stability are desired for HER to scale-up such clean energy technologies.[7−9]

With a hydrogen-binding energy approximate to that of Pt, molybdenum disulfide (MoS_2) displays a good activity in HER from water, and the earth-abundance and economic-cost significantly ensure it as one of the promising substitutes for high-cost Pt catalysts.[6−8,10] The pioneering work of Chorkendorff has demonstrated that the (010) and (100) planes of MoS_2 exposing unsaturated Mo- and S-edges are active for HER, whereas the basal plane of (002) is inert.[11] Motivated by this understanding, intense research efforts have been focused on the surface engineering of nanosized MoS_2 to maximize the number of exposed edge sites.[7,12−15] For example, MoS_2 with rich edge-sites can be achieved on an ordered double-gyroid network with nanopores via hard-templating processes.[16] And 1T-MoS_2 monolayers with intrinsically promoted edge-sites can be obtained through chemical and electrochemical exfoliation of 2H-MoS_2 bulks, via which new active sites are even created on the basal planes due to crystal-strain.[17−20] However, the above strategies suffer fussy procedures or rigid manipulation expelling O_2 and water. Moreover, although hydro/solvothermal processes provide a facile achievement to various nanostructured MoS_2,[21−24] the desired exposure of edge-sites is usually absent because the (010) and (100) planes with high surface energy tend to vanish, leaving inert (002) exposed.[6] This highlights the importance of protecting active sites via the rich interactions during hydro/solvothermal synthesis.

Herein, we propose a reactant-protecting strategy to achieve rich active sites on MoS_2 through a microwave (MW) assisted hydrothermal route, as shown in Scheme 1. Enhanced by MW

Received: August 31, 2015
Accepted: October 8, 2015
Published: October 8, 2015

DOI: 10.1021/acsami.5b08103
ACS Appl. Mater. Interfaces 2015, 7, 23741−23749

Scheme 1. Schematic Illustration for the MW-Assisted Reactant-Protecting Strategy

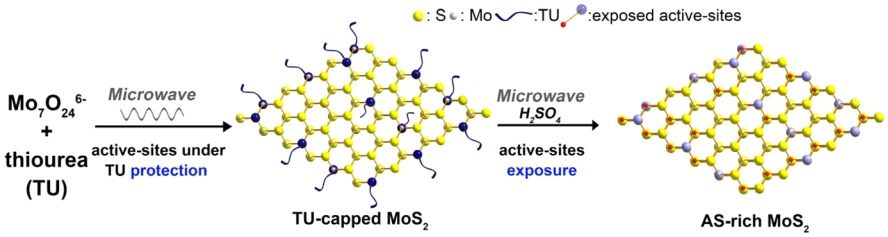

irradiation, the capping of excessive thiourea (TU) on in situ formed MoS_2 (denoted as TU-capped MoS_2) effectively protects the active planes during crystal growth. After the following treatment with diluted H_2SO_4, TU capping is removed, resulting in active-site-rich MoS_2 (denoted as AS-rich MoS_2) nanosheets. In this strategy, MW irradiation accelerates the synthesis of MoS_2 to several minutes owing to the special heating via dipolar polarization and ionic conduction.[25,26] And, TU acts not only as a reactant but also as a capping agent for protecting active sites, avoiding the complicated control and fussy procedure associated with additional surfactants and templates.[27] As a result, such AS-rich MoS_2 delivers an excellent HER activity with a high current density of 68 mA cm^{-2} (at η = 300 mV), a low η_{10} (overpotential required to reach a current of −10 mA cm^{-2}) of 220 mV, a low Tafel slope of 53.5 mV dec^{-1}, and a low η_{onset} (overpotential referring to the beginning of linear regime in Tafel plot) of 180 mV, outperforming those of MoS_2 fabricated by conventional hydrothermal methods.[28−31] As further compared with the edge-terminated MoS_2 derived from fussy templating, mechanically activated annealing, electro-polymerization and electrochemical Li-intercalation procedures,[16,32−34] our AS-rich MoS_2 possessing the comparable electrocatalytic activity is highlighted by its facile synthesis with dramatically reduced reaction time. This work further reveals that the effective protection and good exposure of active sites are indispensable to access active MoS_2 catalysts, verifying the reactant-protecting mechanism.

RESULTS AND DISCUSSION

Through a typical MW-assisted hydrothermal process, TU-capped MoS_2 is fabricated by reacting ammonium heptamolybdate with excessive TU (n_s/n_{Mo} = 12.0) at 220 °C for only 10 min, and after the following treatment with 0.05 M H_2SO_4 at 150 °C, the AS-rich MoS_2 nanosheets are finally received. Figures 1a, b show the scanning electronic microscopy (SEM) images of TU-capped MoS_2 and AS-rich MoS_2. Similar nanosheets with a lateral size of 200−300 nm are observed in both TU-capped MoS_2 and AS-rich MoS_2, confirming the well-retained morphology after H_2SO_4 treatment. In their transition electronic microscopy (TEM) images (Figure 1c, d), the lattice fringes of 0.27 nm can be indexed as the (100) or (010) of hexagonal MoS_2. And the corresponding fast Fourier transform (FFT) patterns, showing irregular diffraction rings, suggest the disordered arrangement of nanodomains on both nanosheets with abundant defects.[22,35,36] Moreover, TU-capped MoS_2 shows a larger interlayer spacing of 0.92 nm (Figure 1c), in contrast to that of 0.62 nm in AS-rich MoS_2 with typical hexagonal phase (Figure 1d). Obviously, a structural evolution is indicated from TU-capped MoS_2 to final AS-rich MoS_2 nanosheets.

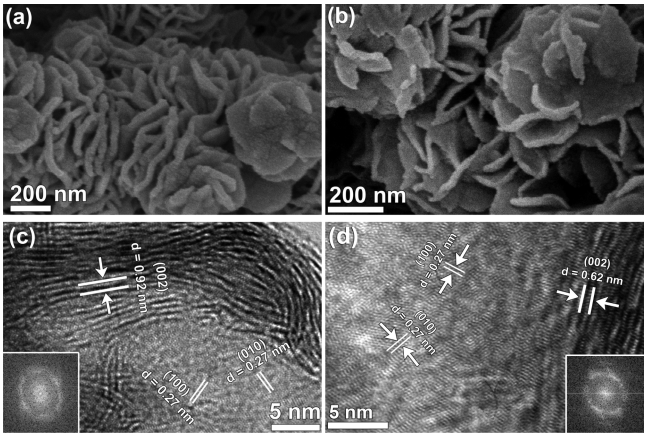

Figure 1. (a, b) SEM and (c, d) TEM images of (a, c) TU-capped MoS_2 and (b, d) AS-rich MoS_2 nanosheets. Insets of c and d are the FFT patterns obtained on nanosheets.

The structural evolution from TU-capped MoS_2 to AS-rich MoS_2 nanosheets, related to TU removal, was further investigated by X-ray diffraction (XRD), Fourier Transform Infrared (FT-IR) and thermogravimetric analysis coupling with differential scanning calorimeter (TGA/DSC) analysis. Figure 2a shows the XRD patterns of the TU-capped MoS_2 and the AS-rich MoS_2 for comparison. Besides the characteristic diffraction peaks assigned to (100), (102) and (110) of hexagonal MoS_2 (JCPDS No. 37−1492), a shifted peak (2θ = 9.64°, d = 9.16 Å) associated with the expanded (002) d-spacing is observed in TU-capped MoS_2. It disappears in AS-rich MoS_2, and instead of that, the peak attributed to typical MoS_2 (002) emerges. This is in accordance with the observation by TEM (Figures 1c, d). Furthermore, their FT-IR spectra illustrate the corresponding evolution in composition (Figure 2b). TU-capped MoS_2 displays the absorption bands associated with $\nu_{C=S}$ (1400 cm^{-1}), ν_{C-N} (1108 cm^{-1}) and δ_{N-H} (619 cm^{-1}), which are absent in AS-rich MoS_2, demonstrating the removal of TU by H_2SO_4 under MW-irradiation ($CS(NH_2)_2 + H_2SO_4 = 2SO_2 + N_2 + CO_2 + 3H_2O$). Accordingly, in TGA/DSC curves (Figure 2c), TU-capped MoS_2 presents an obvious weight loss and two endothermic peaks in the range of 280−350 °C due to the decomposition of adsorbed TU. In comparison with the easier decomposition of free TU (175−245 °C, Figure S1), this delayed decomposition implies strong interactions between TU and MoS_2 in TU-capped MoS_2. Because of the successful removal of TU by diluted H_2SO_4, the above evolution is negligible in AS-rich MoS_2. Noticeably, the similar exothermic reactions around 250−260 °C in their DSC curves are probably associated with the conversion of high-surface-energy planes to stable ones upon heating.

DOI: 10.1021/acsami.5b08103
ACS Appl. Mater. Interfaces 2015, 7, 23741−23749

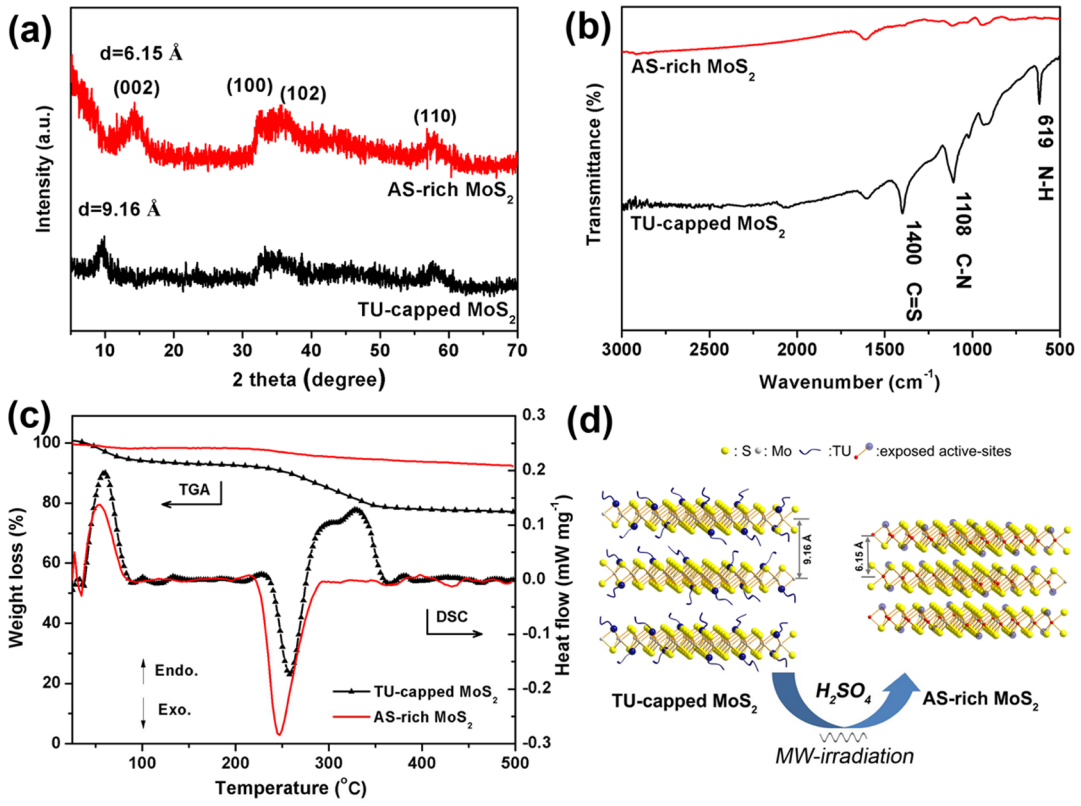

Figure 2. (a) XRD patterns, (b) FT-IR spectra, (c) TGA/DSC curves of TU-capped MoS_2 and AS-rich MoS_2 nanosheets, and (d) schematic structural evolution from TU-capped MoS_2 to AS-rich MoS_2.

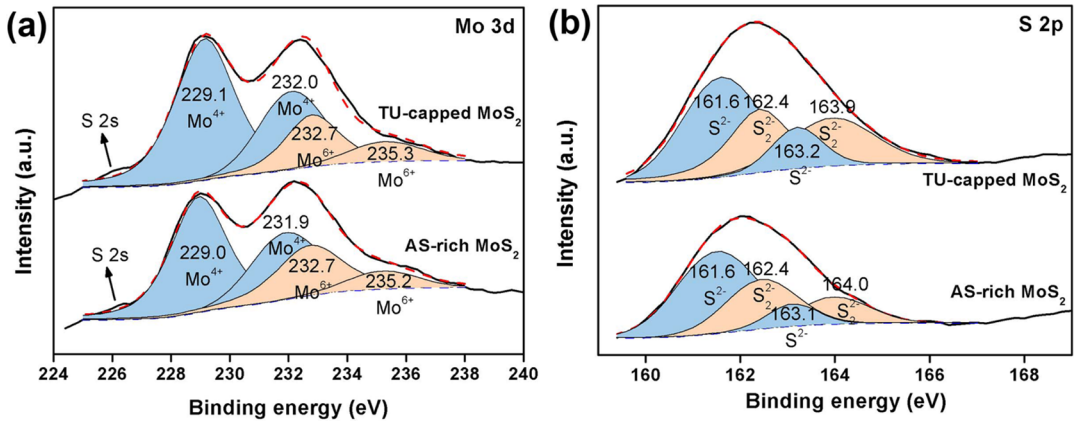

Figure 3. XPS profiles of (a) Mo 3d and (b) S 2p in TU-capped MoS_2 and AS-rich MoS_2 nanosheets.

Obviously, TU can be integrated with MoS_2, and then removed by the treatment with diluted H_2SO_4. Regarding the high surface energy of (100) and (010) planes in MoS_2,[6] it is reasonable to assign most of the TU protection to edge-sites (Figure 2d). Not only that, the observably enlarged interlayer spacing (d = 9.16 Å) in TU-capped MoS_2 further implies that some of TU intercalates into S−Mo−S layers, which is similar to the founding in interlayer-expanded MoS_2 (d = 9.4 Å) intercalated by oxidized *N,N*-dimethylformamide species.[37] However, it is different from recent work reporting expanded interlayers in hydrothermally prepared MoS_2.[22,38,39] Xie et al. ascribed a large interlayer spacing of d = 9.5 Å to oxygen incorporation,[22] in which the absence of TU was confirmed by IR and TGA investigations. Meanwhile, it is reported by other groups that the intercalation of NH_4^+-cation will expand the interlayer spacing of MoS_2.[38,39] To determine the state of N in TU-capped MoS_2, we performed X-ray photoelectron spectra (XPS) analysis (Figure S2). The N 1s binding-energy of 399.8 eV is close to that of alkylamine (399.6 eV), but far from that of ammonium (402.4 eV),[40,41] indicating the presence of TU but not NH_4^+. This further confirms the TU intercalation into S−Mo−S layers of TU-capped MoS_2 (Figure 2d) due to the interactions between TU and the sites on basal planes. And, extra active sites (e.g., defects) beyond edges can be even created after TU removal.

Moreover, the chemical states of Mo and S in both TU-capped MoS_2 and AS-rich MoS_2 are analyzed by XPS measurement. As shown in Figure 3, the coincident XPS peaks of Mo $3d_{3/2}$, Mo $3d_{5/2}$, S $2p_{1/2}$, and S $2p_{3/2}$ in the both two samples verify the similar chemical environment of Mo and

DOI: 10.1021/acsami.5b08103
ACS Appl. Mater. Interfaces 2015, 7, 23741−23749

S before and after TU removal. In Mo 3d profiles (Figure 3a), the peaks at 229.0 ± 0.1 and 232.0 ± 0.1 eV are ascribed to $3d_{5/2}$ and $3d_{3/2}$ of Mo^{4+}, respectively.[42] And those located at 232.7 and 235.2 eV are associated with Mo^{6+} resulting from the surface oxidation of MoS_2 in air. The small satellite-peak around 226.1 corresponds to 2s of S species.[23] Meanwhile, the peaks at 161.6 ± 0.1 and 163.2 ± 0.1 eV in the both of TU-capped MoS_2 and AS-rich MoS_2 are assigned the $2p_{3/2}$ and $2p_{1/2}$ of S^{2-} (Figure 3b).[23,42] The visible ones for S $2p_{3/2}$ (162.4 eV) and S $2p_{1/2}$ (163.9 eV) indicate the presence of bridging S_2^{2-}, which are related to the well-maintained active sites.[23]

To investigate the reactant-protecting strategy toward improved electrocatalytic HER performance, we modified TU-capped MoS_2 and AS-rich MoS_2 onto glassy carbon electrodes (GCEs) for test in 0.5 M H_2SO_4 solution using a typical three-electrode setup. Figure 4a displays the polarization

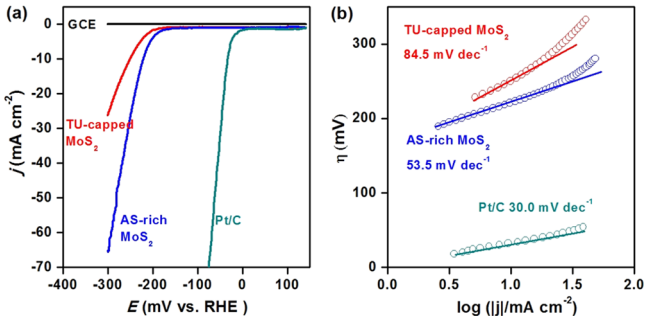

Figure 4. (a) Polarization curves with the scan rate of 2 mV s^{-1} in 0.5 M H_2SO_4, and (b) the corresponding Tafel plots of TU-capped MoS_2, AS-rich MoS_2, and Pt/C (40% Pt on carbon black from Johnson Matthey), with a loading mass of 0.285 mg cm^{-2}.

curves of TU-capped MoS_2 and AS-rich MoS_2 with *iR*-drop corrections, along with the performance of the benchmark Pt/C catalyst. The featureless polarization curve for bare GCE guarantees a minimal background. Remarkably, AS-rich MoS_2 presents a well-improved activity, as compared with TU-capped MoS_2. To achieve a current density of 10 mA cm^{-2}, they require a η_{10} of 220 and 255 mV, respectively. At η = 300 mV, the current density of 68 mA cm^{-2} delivered by AS-rich MoS_2 is nearly three times as high as that by TU-capped MoS_2 (26 mA cm^{-2}).

Tafel plot is a useful metric to assess the HER performance of electrocatalysts and at the same time is an available indicator of the reaction mechanism.[43−45] As displayed in Figure 4b, a η_{onset} of 180 mV and a Tafel slop of 53.5 mV dec^{-1} are observed on AS-rich MoS_2, which are respectively lower than those for TU-capped MoS_2 (225 mV and 84.5 mV dec^{-1}). The small Tafel slope of AS-rich MoS_2 indicates a fast increase of hydrogen generation rate with the applied overpotential, corresponding to the high activity presented in the polarization curves. According to the classic theory, HER in acidic aqueous media proceeds in two steps (eqs 1−3),[7,44] where the * indicates the active site of MoS_2, and H* a hydrogen atom bound to an active site. The first one is a discharge step (Volmer reaction) with a Tafel slope of 118 mV dec^{-1} (eq 1), and the second one is either the ion and atom reaction (Heyrovsky reaction) with a slope of 40 mV dec^{-1} (eq 2) or the atom combination reaction (Tafel reaction) with a slope of 30 mV dec^{-1} (eq 3).[7,10,44] Although the Tafel slope alone is insufficient to determine the specific mechanism, the evidently reduced slope on AS-rich MoS_2 (53.5 mV dec^{-1}), as compared with that on TU-capped MoS_2 (84.5 mV dec^{-1}), still confirms the promoted Volmer step in HER kinetics.[42] In this way, the Volmer reaction as the rate-determining step can be eliminated on AS-rich MoS_2.

$$H_3O^+(aq) + e^- + * \rightarrow H^* + H_2O(l) \quad (1)$$

$$H_3O^+(aq.) + e^- + H^* \rightarrow * + H_2(g) + H_2O(l) \quad (2)$$

$$H^* + H^* \rightarrow 2^* + H_2(g) \quad (3)$$

As compared with that of TU-capped MoS_2, the obviously improved HER performance in AS-rich MoS_2 confirms the function of reactant-protecting under MW irradiation, which stems from the well-retaining active sites. The accurate measurement of the effective electrochemically active surface area (ECSA) is difficult owing to its unclear capacitive behavior. Because the double-layer capacitances (C_{dl}) is linearly proportional to ECSA, an alternative way to calculate C_{dl} is utilized in many previous reports,[17,22,37,46] providing a relative comparison. In this work, cyclic voltammograms (CV, Figure S3) were taken in the region of 150−350 mV vs RHE, in which CV responses mostly results from the charging of double-layer. And, the C_{dl} value can be estimated by plotting the $\Delta J/2$ at 250 mV vs RHE against the scan rate, where the slope is the C_{dl}. The obviously increased C_{dl} of 25.7 mF cm^{-2} is presented by AS-rich MoS_2 nanosheets (Figure 5a), three times of that by

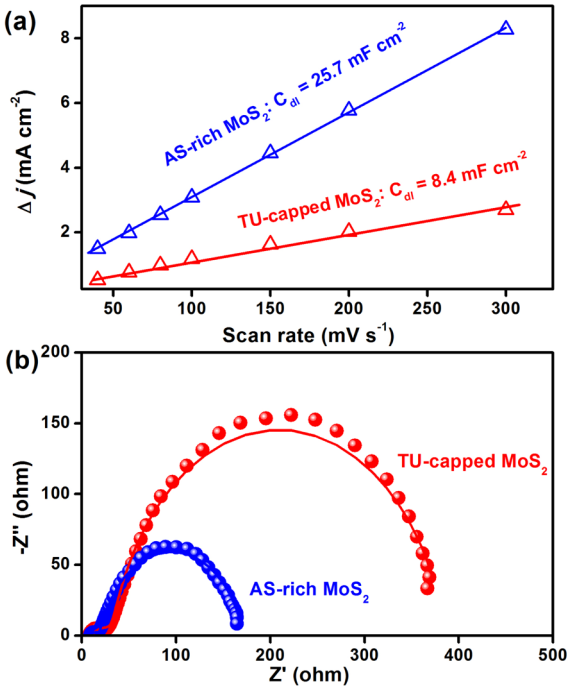

Figure 5. (a) Estimation of C_{dl} by plotting the current density variation ($\Delta j = (j_a - j_c)/2$, at 250 mV vs RHE; data obtained from the CV in Figures S3a, b) against scan rate to fit a linear regression, and (b) Nyquist plots (at η = 200 mV) of TU-capped MoS_2 and AS-rich MoS_2 catalysts.

TU-capped MoS_2 (8.4 mF cm^{-2}). This indicates the high exposure of active surface via MW-assisted reactant-protecting strategy. Furthermore, electrochemical impedance spectroscopy (EIS) analysis was also applied to study the electrode kinetics during HER process. As shown in the Nyquist plots (Figure 5b), AS-rich MoS_2 has a smaller charge transfer resistance (R_{ct})

DOI: 10.1021/acsami.5b08103
ACS Appl. Mater. Interfaces 2015, 7, 23741−23749

of 165.5 Ω than that of TU-capped MoS_2 (395.5 Ω), indicating the fast Faradaic process and thus a high HER activity. The obviously reduced R_{ct} on AS-rich MoS_2 can be ascribed to the removal of TU molecules, which are insulating and hinder the electron transfer in MoS_2 nanocatalysts. In addition, a control experiment fabricating MoS_2 without TU protection further verifies the above function of reactant-protecting toward a high activity on MoS_2. Such MoS_2 nanosheets, which are directly synthesized from reacting AHM with TU ($R_{S/Mo}$ = 12.0) in 0.05 M H_2SO_4 under the same MW condition, only display a low HER activity due to the eliminated TU protection by H_2SO_4 (Figure S4).

Moreover, the long-term stability of AS-rich MoS_2 and the ability to continuously catalyze the generation of H_2 was examined using cycling continuously for 1000 cycles and chronoamperometry, as shown in Figure 6. At the end of the

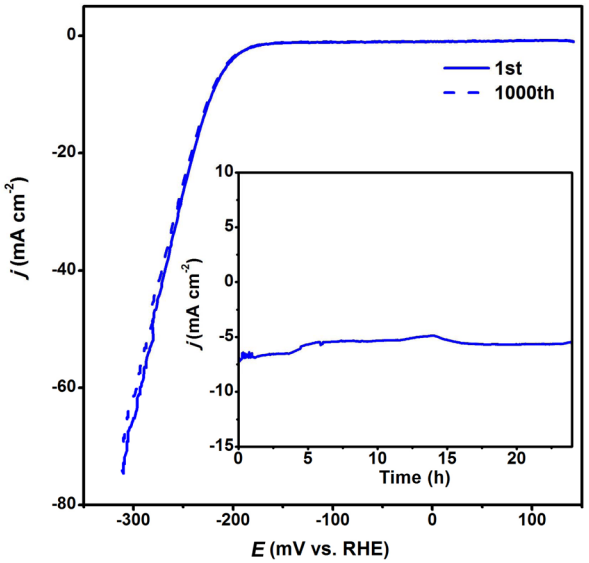

Figure 6. Polarization curves recorded from AS-rich MoS_2 with a sweep rate of 10 mV s^{-1} before and after 1000 potential cycles between −300 and 150 mV vs RHE. The inset shows the time dependence of catalytic currents during electrolysis for AS-rich MoS_2 in 0.5 M H_2SO_4 at −195 mV vs RHE.

cycling procedure, the catalyst affords similar $j-V$ curves to the initial cycle with negligible loss of the cathodic current. As been further evaluated by prolonged electrolysis at a fixed potential (−195 mV vs RHE, inset of Figure 6), the current density of AS-rich MoS_2 generally remains stable in 0.5 M H_2SO_4 for 24 h.

Remarkably, the as-received AS-rich MoS_2 exhibits a good HER activity featured by a high current density of 68 mA cm^{-2} (η = 300 mV), a low η_{10} of 220 mV, a low Tafel slope of 53.5 mV dec^{-1}, and a low η_{onset} of 180 mV, comparing favorably with the reported MoS_2-only catalysts (Table S1). In particular, the η_{10} of AS-rich MoS_2 (220 mV) is obviously lower than those of $V_{0.09}Mo_{0.91}S_2$ nanosheets (ca. 230 mV),[47] MoS_2 quantum/nano dots (~250 mV),[48,49] ammoniated MoS_2 (325 mV)[38] and MoS_2 nanoflowers (275 mV).[29] The HER activity of our AS-rich MoS_2 can be also confirmed by the high current density of AS-rich MoS_2 (68 mA cm^{-2}) at η = 300 mV. However, AS-rich MoS_2 present the moderate Tafel slope and onset overpotential among the previously reported MoS_2,[16,17,29,32−34,38,47−49] which is probably associated with the various mass loading of electrocatalysts (0.013−0.285 mg cm^{-2}). Because the precise analysis of electronic transport for proton reduction can be masked by the multiple proton-coupled electron transfer reactions, Tafel analysis based on polarization curves is highly dependent on the scalability of catalyst use (i.e., increased resistance in thicker catalyst films).[50,51]

Our work presents a new route toward active MoS_2 electrocatalysts for HER, distinguishing from the previous reports. Xie et al. have conducted hydrothermal synthesis employing excessive TU to fabricate defect-rich and oxygen-incorporated MoS_2, which are directly used as efficient HER electrocatalysts.[22,24] The excessive TU can create abundant defect-based active sites on MoS_2,[24] and even balance the number of active sites and electrical conductivity toward prominent HER activity.[22] And, Sun et al. recently reported a MW-assisted strategy for synthesizing MoS_2 with an edge-terminated structure and an expanded interlayer spacing.[37] The expansion of interlayers due to the intercalating *N*,*N*-dimethylformamide species effectively modifies the electronic structures and electrical conductivity of MoS_2 edge sites, resulting in superior performance for electrochemical HER. Different from the above reports, the TU-capped MoS_2 in this work only presents a low HER activity owing to TU-capping on active sites, whereas AS-rich MoS_2 is highly active after TU removal. This indicates another mechanism, i.e., reactant-protecting promoted by MW irradiation.

To elucidate the reactant-protecting mechanism toward highly exposed active sites on MoS_2 electrocatalysts, a series of control experiments have been further conducted. It is found that the effective adsorption of capping agents and their successful removal are the key factors, which are associated with the protection and exposure of active sites, respectively.

MW-irradiation is indispensable in this reactant-protecting strategy. We examined a typical hydrothermal synthesis employing the same conditions of MW-assisted procedures to fabricate MoS_2. The products before and after H_2SO_4 treatment are denoted as TU-capped MoS_2−HT and MoS_2−HT ("HT" stands for "hydrothermal"), respectively, which present the similar morphology of nanosheets (Figure S5) to those derived from MW-assisted routes. Both of them only present a poor HER activity in the polarization curves (Figure 7a), with slight increase after H_2SO_4 treatment. In comparison with the active AS-rich MoS_2 derived from MW routes, TU-capped MoS_2−HT and MoS_2−HT displays the low current density of 9 and 11 mA cm^{-2} at η = 300 mV, respectively, and their Tafel slopes of 90.1 and 87.5 mV dec^{-1} indicate the poor kinetic behaviors. It can be explained by their low electrochemical C_{dl} and large R_{ct} (Figure 7b, c). As ascertained by CHN elemental analysis, the content of N (0.9 wt %) in TU-capped MoS_2−HT is obviously lower than that of TU-capped MoS_2 (3.5 wt %, Figure S6). It is suggested that the TU protection is insufficient in hydrothermal synthesis. Therefore, the successful reactant-protecting strategy toward highly active MoS_2 electrocatalysts should be reasonably ascribed to the special heating by MW-irradiation on the basis of dipolar polarization and ionic conduction,[26] which prefers the formation of Mo−S polar bonds and consequently enhances the adsorption of TU on MoS_2.

Furthermore, the feeding ratio of n_S/n_{Mo} ($R_{S/Mo}$) makes an obvious influence on the activity of final AS-rich MoS_2 nanosheets received after the successful removal of TU (c.f. polarization curves in Figure S7). To conveniently illustrate the different promotion in activity, the current densities at η = 300 mV are compared in Figure 8a, the same as the following discussion in the treatment for TU removal (Figure 8b). As

DOI: 10.1021/acsami.5b08103
ACS Appl. Mater. Interfaces 2015, 7, 23741−23749

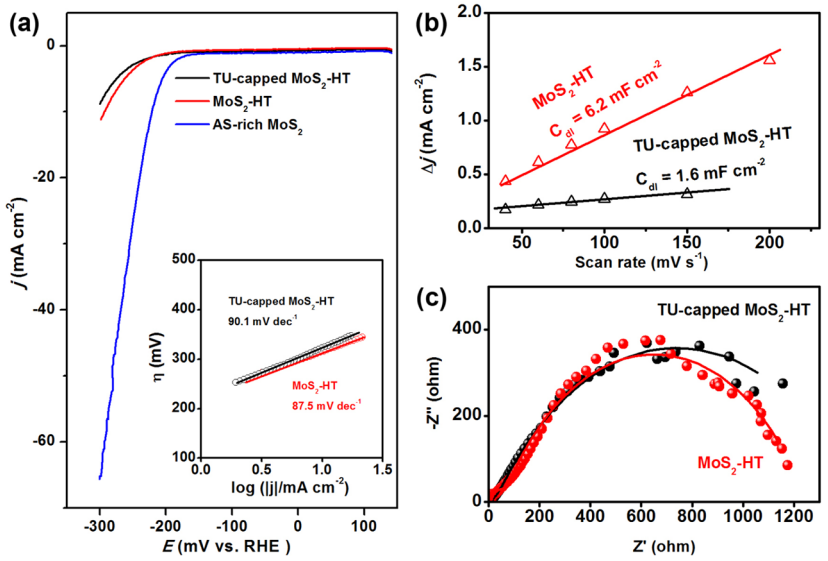

Figure 7. (a) Polarization curves with the scan rate of 2 mV s^{-1} in 0.5 M H_2SO_4, and (inset of a) the corresponding Tafel plots of MoS_2 derived from typical hydrothermal processes. (b) C_{dl} estimated by plotting the current density variation ($\Delta j = (j_a - j_c)/2$) at 250 mV vs RHE (data obtained from Figures S3c, d) against scan rate, and (c) Nyquist plots (η = 200 mV) of TU-capped MoS_2–HT and MoS_2–HT.

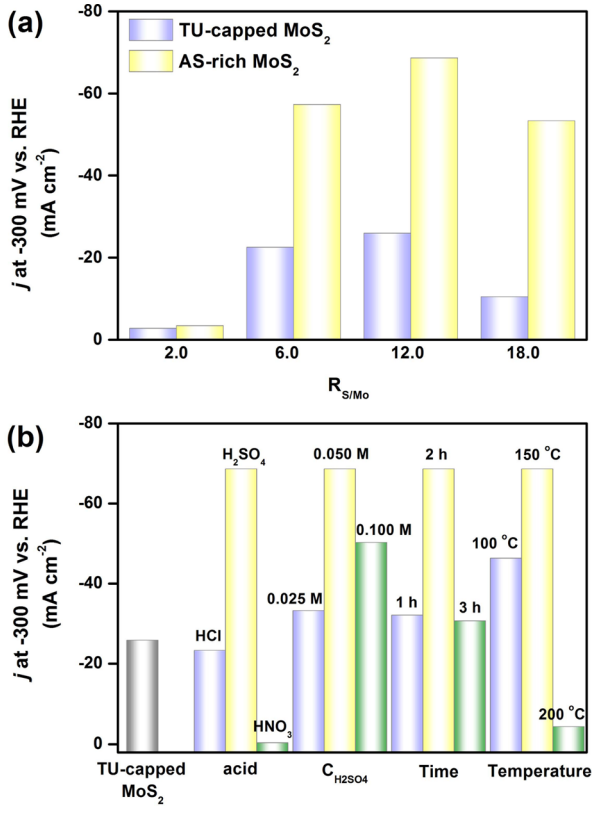

Figure 8. HER activity over various TU-capped MoS_2 and AS-rich MoS_2 nanosheets derived from varying (a) feeding $R_{S/Mo}$ in the first synthetic step and (b) treating condition for removing adsorbed TU. The activity is featured by the current density at η = 300 mV in 0.5 M H_2SO_4.

shown in Figure 8a, the poor activity with a low current density of 3 mA cm^{-2} is observed on AS-rich MoS_2 nanosheets when a low $R_{S/Mo}$ of 2.0 is adopted, without obvious improvement in comparison with TU-capped MoS_2. This is due to the insufficient TU for MoS_2 generation and effective protection on active sites, as indicated by its XRD pattern showing the remaining phase of $(NH_4)_2Mo_3O_{10}$ (Figure S8). With TU feeding increased to $R_{S/Mo}$ = 6.0, the obviously improved activity is well presented on MoS_2, in which the current density of 57 mA cm^{-2} at η = 300 mV is more than twice of that on TU-capped MoS_2 (23 mA cm^{-2}). And the highest activity with a current density of 68 mA cm^{-2} is achieved with $R_{S/Mo}$ of 12.0. Because the highly excessive TU with strong interactions would even disturb the crystallization of MoS_2 at $R_{S/Mo}$ = 18.0 (c.f. XRD patterns in Figure S8), the activity is a bit lower than the case with $R_{S/Mo}$ of 12.0. Nevertheless, the improvement related to the recovery of active sites is still visible.

A suitable treatment is crucial to successfully remove the adsorbed TU molecules while retain the active sites. We have demonstrated that the diluted H_2SO_4 (0.05 M) with mild oxidizability can drive TU decomposition, without destroying the structure of MoS_2. In comparison, no improvement in HER activity is observed (Figure 8b and Figure S9) after the treatment with HCl (0.1 M), which should be ascribed to the failure in TU removal due to the weak oxidizability of HCl (Figure S10). On the contrary, HNO_3 (0.1 M) is so strong in oxidation that only the oxidized product of MoO_3 with a poor HER activity is received (Figure 8b and Figures S9 and S10). Besides, the HER activity also depends on the concentration of H_2SO_4, treating time, and reaction temperature in control experiments (Figure 8b and Figure S9), suggesting an optimized treatment (C_{H2SO4} = 0.050 M, t = 2.0 h, and T = 150 °C) for fully exposed active sites without any damage. Furthermore, the removal of capping agents to recover the active sites of MoS_2 is also associated with the molecular structure of S-containing reactants. The improvement in activity is visible with thioacetamide (TAA, Figure S11), but is negligible with L-cysteine (L-cys). FT-IR spectra clearly identify the successful removal of TAA after H_2SO_4 treatment, but failure in the case of L-cys (Figure S11), interpreting the difference in HER performance. The strong interactions between L-cys and MoS_2, prohibiting the removal of adsorbed L-cys, should be ascribed to the multiple function groups of −SH, $-NH_2$, and −COOH.

DOI: 10.1021/acsami.5b08103
ACS Appl. Mater. Interfaces 2015, 7, 23741−23749

Additionally, the MW-assisted reactant-protecting strategy can be extended to supported MoS_2 catalysts. On the conducting supports of CNTs and RGO, the structural evolution associated with TU adsorption and removal is visible (Figure S12). The further promoted HER performance is achieved on such supported MoS_2 catalysts. Remarkably, MoS_2/CNTs and MoS_2/RGO with rich active sites present the high current density of 7.0 and 10.6 mA cm^{-2} μg_{MoS2}^{-1} at η = 300 mV, respectively, which is higher than that on bare AS-rich MoS_2 (3.3 mA cm^{-2} μg_{MoS2}^{-1}).

CONCLUSION

In this paper, we introduced a new MW-assisted reactant-protecting strategy to fabricate highly active MoS_2 with rich active sites, employing the enhanced adsorption of excessive TU on MoS_2 by MW. The AS-rich MoS_2 nanosheets presents a superior HER activity characterized by a high current density of 68 mA cm^{-2} (η = of 300 mV), a low η_{10} of 220 mV, a low tafel slope of 53.5 mV dec^{-1}, and a low η_{onset} of 180 mV. For achieving efficient MoS_2 catalysts, TU capping, and removal are further demonstrated crucial in a series of control experiments. This work provides a feasible strategy toward active-site-rich catalysts via interface engineering, opening up new opportunities for developing high-performance nanomaterials in energy field.

EXPERIMENTAL SECTION

Materials. Ammonium heptamolybdate tetrahydrate ($(NH_4)_6Mo_7O_{24}\bullet 4H_2O$), thiourea ($CS(NH_2)_2$), thioacetamide ($CH_3CSNH_2$), and L-cysteine ($C_3H_7NO_2S$) were purchased from Sinopharm Chemical Reagent Co. Ltd. (Shanghai, China). Carbon nanotubes and graphene oxide nanosheets were provided by Nanotech Port (Shenzhen, China) and XFNANO (Nanjing, China), respectively. And Nafion solution (5 wt % in lower aliphatic alcohols and water) was purchased from Sigma-Aldrich.

Catalyst Preparation. AS-rich MoS_2 nanosheets were synthesized as following: ammonium heptamolybdate tetrahydrate ($(NH_4)_6Mo_7O_{24}\cdot 4H_2O$) and TU were dissolved in 15.0 mL of distilled water, and then the solution was turned to a microwave reactor (Preekem MX-8000, Shanghai). After MW irradiation at 220 °C for 10 min, the as-received TU-capped MoS_2 was collected by centrifugation, thoroughly washed with distilled water for three times, dried at 50 °C. And then, the AS-rich MoS_2 nanosheets were finally harvested after the treatment with diluted H_2SO_4 (0.05 mol L^{-1}) under MW at 150 °C for 2 h. As for the control experiments to hydrothermally synthesize TU-capped MoS_2–HT and MoS_2–HT (HT stands for "hydrothermal"), the process was carried out via the similar procedures: 0.35 g of AHM was dissolved in 15.0 mL of H_2O containing 1.83 g of thiourea ($R_{S/Mo}$ = 12.0), which were then transferred to a Teflon-lined stainless-steel autoclave and treated at 220 °C for 24 h. After that, the product was treated with 0.05 mol L^{-1} H_2SO_4 under MW-irradiation at 150 °C for 2 h.

As for supported MoS_2 electrocatalysts, CNTs and GO were employed as the supports. Typically, 0.13 g of CNTs or GO was dispersed in 15.0 mL of H_2O containing 0.35 g of AHM and 1.83 g of TU ($R_{S/Mo}$ = 12.0), and then was processed via the same procedures as those for fabricating AS-rich MoS_2 nanosheets.

Physical Measurement. SEM and TEM investigations were taken on a ZEISS ULTRA55 and a JEOL JEM 2100F, respectively. XRD analysis was performed on Bruker D8 diffractometer using Cu Kα radiation (λ = 1.54056 Å). XPS was processed on a PerkineElmer PHI5000c XPS, using C 1s (B. E. = 284.6 eV) as a reference. TGA/DSC was tested on NETZSCH STA449F3 under N_2 flow. FT-IR spectra were collected with a Nicolet 6700 FTIR spectrometer. The N content in a series of MoS_2 samples was determined by CHN elemental using a Vario EL Elementar. To determine MoS_2 loading in MoS_2/CNTs and MoS_2/RGO, the Mo elemental analysis was performed by an inductively coupled plasma-atomic emission spectroscopy (ICP-AES).

Electrochemical HER Test. MoS_2-based nansheets were modified onto a glassy carbon electrode (GCE) for test in 0.5 mol L^{-1} H_2SO_4 solution using a typical three-electrode setup. Typically, 4 mg of catalyst and 40 μL of 5 wt % Nafion solution were dispersed in 1 mL of 4:1 v/v water/ethanol by at least 30 min sonication to form a homogeneous ink. Then 5 μL of the catalyst ink was loaded onto a GCE of 3 mm in diameter, resulting in the mass loading of 0.285 mg cm^{-2}. Linear sweep voltammetry (LSV) was conducted with the scan rate of 2 mV s^{-1} in 0.5 mol L^{-1} H_2SO_4 on a potentiostat of CHI760 (CH Instruments), using a saturated calomel electrode as the reference electrode, and a graphite electrode as the counter electrode. All the potentials reported in this work were referenced to a reversible hydrogen electrode (RHE) by adding a value of (0.241 + 0.059 pH) V. AC impedance measurements were carried out in the same configuration at η = 200 mV from 1 × 10^6 to 0.01 Hz with an AC voltage of 5 mV.

ASSOCIATED CONTENT

Supporting Information

The Supporting Information is available free of charge on the ACS Publications website at DOI: 10.1021/acsami.5b08103.

TGA/DSC curve of TU, N 1s XPS profile of TU-capped MoS_2, SEM image and XRD pattern of MoS_2 synthesized without TU protection, SEM and TEM images of TU-capped MoS_2–HT and MoS_2–HT, CV and elemental analysis results of TU-capped MoS_2 and AS-rich MoS_2, and LSV of various MoS_2 catalysts (PDF)

AUTHOR INFORMATION

Corresponding Authors

*E-mail: mslcyang@scut.edu.cn.

*E-mail: tqsgao@jnu.edu.cn.

Author Contributions

†N.L. and Y.G. contributed equally to this work.

Notes

The authors declare no competing financial interest.

ACKNOWLEDGMENTS

This work is supported by National Basic Research Program of China (2013CB934101), National Natural Science Foundation of China (21203075, 21373102, 21433002 and 51402110), and Fundamental Research Funds for the Central Universities (21615402). Q.S.G. also thanks the support from Guangdong Higher Education Institute (YQ2013022) and Guangdong Natural Science Funds (2015A030306014 and 2014TQ01N036).

REFERENCES

(1) Cook, T. R.; Dogutan, D. K.; Reece, S. Y.; Surendranath, Y.; Teets, T. S.; Nocera, D. G. Solar Energy Supply and Storage for the Legacy and Non legacy Worlds. *Chem. Rev.* **2010**, *110*, 6474–6502.

(2) Lewis, N. S.; Nocera, D. G. Powering the Planet: Chemical Challenges in Solar Energy Utilization. *Proc. Natl. Acad. Sci. U. S. A.* **2006**, *103*, 15729–15735.

(3) Mallouk, T. E. Water Eelctrolysis: Divide and Conquer. *Nat. Chem.* **2013**, *5*, 362–363.

(4) Spurgeon, J. M.; Walter, M. G.; Zhou, J.; Kohl, P. A.; Lewis, N. S. Electrical Conductivity, Ionic Conductivity, Optical Absorption, and Gas Separation Properties of Ionically Conductive Polymer Membranes Embedded with Si Microwire Arrays. *Energy Environ. Sci.* **2011**, *4*, 1772–1780.

DOI: 10.1021/acsami.5b08103
ACS Appl. Mater. Interfaces 2015, 7, 23741–23749

(5) Zou, X. X.; Zhang, Y. Noble Metal-free Hydrogen Evolution Catalysts for Water Splitting. *Chem. Soc. Rev.* **2015**, *44*, 5148−5180.
(6) Laursen, A. B.; Kegnaes, S.; Dahl, S.; Chorkendorff, I. Molybdenum Sulfides-Efficient and Viable Materials for Electro- and Photoelectrocatalytic Hydrogen Evolution. *Energy Environ. Sci.* **2012**, *5*, 5577−5591.
(7) Morales-Guio, C. G.; Stern, L. A.; Hu, X. L. Nanostructured Hydrotreating Catalysts for Electrochemical Hydrogen Evolution. *Chem. Soc. Rev.* **2014**, *43*, 6555−6569.
(8) Faber, M. S.; Jin, S. Earth-Abundant Inorganic Electrocatalysts and Their Nanostructures for Energy Conversion Applications. *Energy Environ. Sci.* **2014**, *7*, 3519−3542.
(9) McKone, J. R.; Marinescu, S. C.; Brunschwig, B. S.; Winkler, J. R.; Gray, H. B. Earth-Abundant Hydrogen Evolution Electrocatalysts. *Chem. Sci.* **2014**, *5*, 865−878.
(10) Zeng, M.; Li, Y. G. Recent Advances in Heterogeneous Electrocatalysts for the Hydrogen Evolution Reaction. *J. Mater. Chem. A* **2015**, *3*, 14942−14962.
(11) Jaramillo, T. F.; Jorgensen, K. P.; Bonde, J.; Nielsen, J. H.; Horch, S.; Chorkendorff, I. Identification of Active Edge Sites for Electrochemical H_2 Evolution from MoS_2 Nanocatalysts. *Science* **2007**, *317*, 100−102.
(12) Benck, J. D.; Hellstern, T. R.; Kibsgaard, J.; Chakthranont, P.; Jaramillo, T. F. Catalyzing the Hydrogen Evolution Reaction (HER) with Molybdenum Sulfide Nanonnaterials. *ACS Catal.* **2014**, *4*, 3957−3971.
(13) Yan, Y.; Xia, B. Y.; Xu, Z. C.; Wang, X. Recent Development of Molybdenum Sulfides as Advanced Electrocatalysts for Hydrogen Evolution Reaction. *ACS Catal.* **2014**, *4*, 1693−1705.
(14) Yan, Y.; Ge, X.; Liu, Z.; Wang, J.-Y.; Lee, J.-M.; Wang, X. Facile Synthesis of Low Crystalline MoS_2 Nanosheet-Coated CNTs for Enhanced Hydrogen Evolution Reaction. *Nanoscale* **2013**, *5*, 7768−7771.
(15) Yan, Y.; Xia, B.; Li, N.; Xu, Z.; Fisher, A.; Wang, X. Vertically Oriented MoS_2 and WS_2 Nanosheets Directly Grown on Carbon Cloth as Efficient and Stable 3-Dimensional Hydrogen-Evolving Cathodes. *J. Mater. Chem. A* **2015**, *3*, 131−135.
(16) Kibsgaard, J.; Chen, Z. B.; Reinecke, B. N.; Jaramillo, T. F. Engineering the Surface Structure of MoS_2 to Preferentially Expose Active Edge Sites for Electrocatalysis. *Nat. Mater.* **2012**, *11*, 963−969.
(17) Lukowski, M. A.; Daniel, A. S.; Meng, F.; Forticaux, A.; Li, L. S.; Jin, S. Enhanced Hydrogen Evolution Catalysis from Chemically Exfoliated Metallic MoS_2 Nanosheets. *J. Am. Chem. Soc.* **2013**, *135*, 10274−10277.
(18) Voiry, D.; Salehi, M.; Silva, R.; Fujita, T.; Chen, M. W.; Asefa, T.; Shenoy, V. B.; Eda, G.; Chhowalla, M. Conducting MoS_2 Nanosheets as Catalysts for Hydrogen Evolution Reaction. *Nano Lett.* **2013**, *13*, 6222−6227.
(19) Tan, Y. W.; Liu, P.; Chen, L. Y.; Cong, W. T.; Ito, Y.; Han, J. H.; Guo, X. W.; Tang, Z.; Fujita, T.; Hirata, A.; Chen, M. W. Monolayer MoS_2 Films Supported by 3D Nanoporous Metals for High-Efficiency Electrocatalytic Hydrogen Production. *Adv. Mater.* **2014**, *26*, 8023−8028.
(20) Lee, J. H.; Jang, W. S.; Han, S. W.; Baik, H. K. Efficient Hydrogen Evolution by Mechanically Strained MoS_2 Nanosheets. *Langmuir* **2014**, *30*, 9866−9873.
(21) Yu, X. Y.; Hu, H.; Wang, Y. W.; Chen, H. Y.; Lou, X. W. Ultrathin MoS_2 Nanosheets Supported on N-doped Carbon Nanoboxes with Enhanced Lithium Storage and Electrocatalytic Properties. *Angew. Chem., Int. Ed.* **2015**, *54*, 7395−7398.
(22) Xie, J. F.; Zhang, J. J.; Li, S.; Grote, F.; Zhang, X. D.; Zhang, H.; Wang, R. X.; Lei, Y.; Pan, B. C.; Xie, Y. Controllable Disorder Engineering in Oxygen-Incorporated MoS_2 Ultrathin Nanosheets for Efficient Hydrogen Evolution. *J. Am. Chem. Soc.* **2013**, *135*, 17881−17888.
(23) Yan, Y.; Xia, B. Y.; Ge, X. M.; Liu, Z. L.; Wang, J. Y.; Wang, X. Ultrathin MoS_2 Nanoplates with Rich Active Sites as Highly Efficient Catalyst for Hydrogen Evolution. *ACS Appl. Mater. Interfaces* **2013**, *5*, 12794−12798.
(24) Xie, J. F.; Zhang, H.; Li, S.; Wang, R. X.; Sun, X.; Zhou, M.; Zhou, J. F.; Lou, X. W.; Xie, Y. Defect-Rich MoS_2 Ultrathin Nanosheets with Additional Active Edge Sites for Enhanced Electrocatalytic Hydrogen Evolution. *Adv. Mater.* **2013**, *25*, 5807−5813.
(25) Gawande, M. B.; Shelke, S. N.; Zboril, R.; Varma, R. S. Microwave-Assisted Chemistry: Synthetic Applications for Rapid Assembly of Nanomaterials and Organics. *Acc. Chem. Res.* **2014**, *47*, 1338−1348.
(26) Baghbanzadeh, M.; Carbone, L.; Cozzoli, P. D.; Kappe, C. O. Microwave-Assisted Synthesis of Colloidal Inorganic Nanocrystals. *Angew. Chem., Int. Ed.* **2011**, *50*, 11312−11359.
(27) Cheng, L.; Huang, W.; Gong, Q.; Liu, C.; Liu, Z.; Li, Y.; Dai, H. Ultrathin WS_2 Nanoflakes as a High-Performance Electrocatalyst for the Hydrogen Evolution Reaction. *Angew. Chem., Int. Ed.* **2014**, *53*, 7860−7863.
(28) Zhang, L.; Wu, H. B.; Yan, Y.; Wang, X.; Lou, X. W. Hierarchical MoS_2 Microboxes Constructed by Nanosheets with Enhanced Electrochemical Properties for Lithium Storage and Water Splitting. *Energy Environ. Sci.* **2014**, *7*, 3302−3306.
(29) Wang, D. Z.; Pan, Z.; Wu, Z. Z.; Wang, Z. P.; Liu, Z. H. Hydrothermal synthesis of MoS_2 nanoflowers as highly efficient hydrogen evolution reaction catalysts. *J. Power Sources* **2014**, *264*, 229−234.
(30) Chung, D. Y.; Park, S. K.; Chung, Y. H.; Yu, S. H.; Lim, D. H.; Jung, N.; Ham, H. C.; Park, H. Y.; Piao, Y.; Yoo, S. J.; Sung, Y. E. Edge-exposed MoS_2 Nano-assembled Structures as Efficient Electrocatalysts for Hydrogen Evolution Reaction. *Nanoscale* **2014**, *6*, 2131−2136.
(31) Chen, Z.; Cummins, D.; Reinecke, B. N.; Clark, E.; Sunkara, M. K.; Jaramillo, T. F. Core-shell MoO_3-MoS_2 Nanowires for Hydrogen Evolution: A Functional Design for Electrocatalytic Materials. *Nano Lett.* **2011**, *11*, 4168−4175.
(32) Merki, D.; Fierro, S.; Vrubel, H.; Hu, X. Amorphous Molybdenum Sulfide Films as Catalysts for Electrochemical Hydrogen Production in Water. *Chem. Sci.* **2011**, *2*, 1262−1267.
(33) Wu, Z.; Fang, B.; Wang, Z.; Wang, C.; Liu, Z.; Liu, F.; Wang, W.; Alfantazi, A.; Wang, D.; Wilkinson, D. P. MoS_2 Nanosheets: A Designed Structure with High Active Site Density for the Hydrogen Evolution Reaction. *ACS Catal.* **2013**, *3*, 2101−2107.
(34) Wang, H.; Lu, Z.; Xu, S.; Kong, D.; Cha, J. J.; Zheng, G.; Hsu, P.-C.; Yan, K.; Bradshaw, D.; Prinz, F. B.; Cui, Y. Electrochemical Tuning of Vertically Aligned MoS_2 Nanofilms and Its Application in Improving Hydrogen Evolution Reaction. *Proc. Natl. Acad. Sci. U. S. A.* **2013**, *110*, 19701−19706.
(35) An, J.; Voelkl, E.; Suk, J. W.; Li, X.; Magnuson, C. W.; Fu, L.; Tiemeijer, P.; Bischoff, M.; Freitag, B.; Popova, E.; Ruoff, R. S. Domain (Grain) Boundaries and Evidence of "Twinlike" Structures in Chemically Vapor Deposited Grown Graphene. *ACS Nano* **2011**, *5*, 2433−2439.
(36) Huang, P. Y.; Ruiz-Vargas, C. S.; van der Zande, A. M.; Whitney, W. S.; Levendorf, M. P.; Kevek, J. W.; Garg, S.; Alden, J. S.; Hustedt, C. J.; Zhu, Y.; Park, J.; McEuen, P. L.; Muller, D. A. Grains and Grain Boundaries in Single-Layer Graphene Atomic Patchwork Quilts. *Nature* **2011**, *469*, 389−392.
(37) Gao, M. R.; Chan, M. K. Y.; Sun, Y. G. Edge-Terminated Molybdenum Disulfide with a 9.4-Å Interlayer Spacing for Electrochemical Hydrogen Production. *Nat. Commun.* **2015**, *6*, 7493.
(38) Wu, Z. Z.; Tang, C. Y.; Zhou, P.; Liu, Z. H.; Xu, Y. S.; Wang, D. Z.; Fang, B. Z. Enhanced Hydrogen Evolution Catalysis from Osmotically Swollen Ammoniated MoS_2. *J. Mater. Chem. A* **2015**, *3*, 13050−13056.
(39) Anto Jeffery, A.; Nethravathi, C.; Rajamathi, M. Two-Dimensional Nanosheets and Layered Hybrids of MoS_2 and WS_2 through Exfoliation of Ammoniated MS_2 (M = Mo,W). *J. Phys. Chem. C* **2014**, *118*, 1386−1396.
(40) Gao, Q. S.; Chen, P.; Zhang, Y. H.; Tang, Y. Synthesis and Characterization of Organic-Inorganic Hybrid GeO_x/Ethylenediamine Nanowires. *Adv. Mater.* **2008**, *20*, 1837−1842.

DOI: 10.1021/acsami.5b08103
ACS Appl. Mater. Interfaces 2015, 7, 23741−23749

(41) Luo, B.; Rossini, J. E.; Gladfelter, W. L. Zinc Oxide Nanocrystals Stabilized by Alkylammonium Alkylcarbamates. *Langmuir* **2009**, *25*, 13133−13141.
(42) Liu, N.; Yang, L. C.; Wang, S. N.; Zhong, Z. W.; He, S. N.; Yang, X. Y.; Gao, Q. S.; Tang, Y. Ultrathin MoS_2 Nanosheets Growing within an in-situ-Formed Template as Efficient Electrocatalysts for Hydrogen Evolution. *J. Power Sources* **2015**, *275*, 588−594.
(43) Skulason, E.; Tripkovic, V.; Bjorketun, M. E.; Gudmundsdottir, S.; Karlberg, G.; Rossmeisl, J.; Bligaard, T.; Jonsson, H.; Norskov, J. K. Modeling the Electrochemical Hydrogen Oxidation and Evolution Reactions on the Basis of Density Functional Theory Calculations. *J. Phys. Chem. C* **2010**, *114*, 18182−18197.
(44) Vilekar, S. A.; Fishtik, I.; Datta, R. Kinetics of the Hydrogen Electrode Reaction. *J. Electrochem. Soc.* **2010**, *157*, B1040−B1050.
(45) Conway, B. E.; Tilak, B. V. Interfacial Processes Involving Electrocatalytic Evolution and Oxidation of H_2, and the Role of Chemisorbed H. *Electrochim. Acta* **2002**, *47*, 3571−3594.
(46) Wu, H. B.; Xia, B. Y.; Yu, L.; Yu, X.-Y.; Lou, X. W. Porous molybdenum carbide nano-octahedrons synthesized via confined carburization in metal-organic frameworks for efficient hydrogen production. *Nat. Commun.* **2015**, *6*, 6512.
(47) Sun, X.; Dai, J.; Guo, Y. Q.; Wu, C. Z.; Hu, F. T.; Zhao, J. Y.; Zeng, X. C.; Xie, Y. Semimetallic Molybdenum Disulfide Ultrathin Nanosheets as An Efficient Electrocatalyst for Hydrogen Evolution. *Nanoscale* **2014**, *6*, 8359−8367.
(48) Gopalakrishnan, D.; Damien, D.; Shaijumon, M. M. MoS_2 Quantum Dot-Interspersed Exfoliated MoS_2 Nanosheets. *ACS Nano* **2014**, *8*, 5297−5303.
(49) Benson, J.; Li, M.; Wang, S.; Wang, P.; Papakonstantinou, P. Electrocatalytic Hydrogen Evolution Reaction on Edges of a Few Layer Molybdenum Disulfide Nanodots. *ACS Appl. Mater. Interfaces* **2015**, *7*, 14113−14122.
(50) Liao, L.; Wang, S.; Xiao, J.; Bian, X.; Zhang, Y.; Scanlon, M. D.; Hu, X.; Tang, Y.; Liu, B.; Girault, H. H. A Nanoporous Molybdenum Carbide Nanowire as An Electrocatalyst for Hydrogen Evolution Reaction. *Energy Environ. Sci.* **2014**, *7*, 387−392.
(51) Vrubel, H.; Moehl, T.; Gratzel, M.; Hu, X. L. Revealing and Accelerating Slow Electron Transport in Amorphous Molybdenum Sulphide Particles for Hydrogen Evolution Reaction. *Chem. Commun.* **2013**, *49*, 8985−8987.

DOI: 10.1021/acsami.5b08103
ACS Appl. Mater. Interfaces 2015, 7, 23741−23749